



OPEN

## Angiotensin converting enzyme 2 is a novel target of the $\gamma$ -secretase complex

Alberto Bartolomé<sup>1</sup>, Jiani Liang<sup>1</sup>, Pengfei Wang<sup>2</sup>, David D. Ho<sup>2</sup> & Utpal B. Pajvani<sup>1✉</sup>

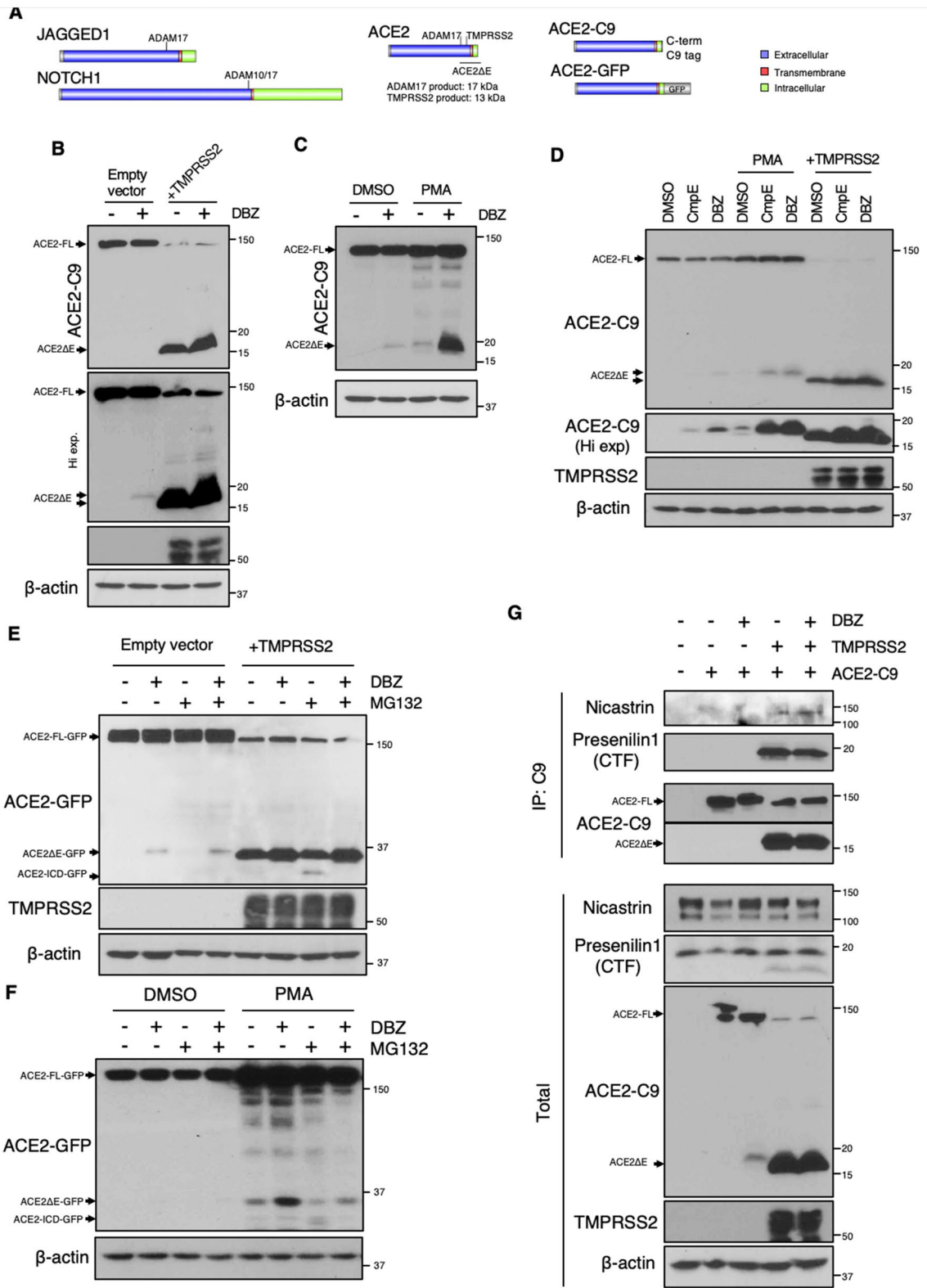
Angiotensin converting enzyme 2 (ACE2) is a key regulator of the renin-angiotensin system, but also the functional receptor of the severe acute respiratory syndrome coronavirus 2 (SARS-CoV-2). Based on structural similarity with other  $\gamma$ -secretase ( $\gamma$ S) targets, we hypothesized that ACE2 may be affected by  $\gamma$ S proteolytic activity. We found that after ectodomain shedding, ACE2 is targeted for intramembrane proteolysis by  $\gamma$ S, releasing a soluble ACE2 C-terminal fragment. Consistently, chemical or genetic inhibition of  $\gamma$ S results in the accumulation of a membrane-bound fragment of ectodomain-deficient ACE2. Although chemical inhibition of  $\gamma$ S does not alter SARS-CoV-2 cell entry, these data point to a novel pathway for cellular ACE2 trafficking.

Angiotensin converting enzyme 2 (ACE2) is a membrane-anchored ectoenzyme that processes Angiotensin II to Angiotensin 1–7, but also mediates the entry of three different coronavirus strains by means of binding the viral spike (S) protein: NL63<sup>1</sup>, SARS-CoV<sup>2</sup> and SARS-CoV-2<sup>3</sup>. S-protein binding to ACE2 triggers membrane fusion and viral entry, but only after S-protein priming by Transmembrane protease serine 2 (TMPRSS2)<sup>3,4</sup>, which also cleaves the ectodomain of ACE2<sup>5</sup>. ACE2 cleavage, or shedding, can additionally be induced by the disintegrin and metallopeptidase domain 17 (ADAM17)<sup>6</sup>, which was found to compete with TMPRSS2<sup>5</sup>. In this regard, there are conflicting reports of ADAM17-mediated shedding affecting SARS-CoV entry<sup>5,7</sup>. Viral infection has also been shown to trigger ACE2 endocytosis<sup>8</sup>, leading to reduced cell surface expression of ACE2<sup>9</sup>. Intriguingly, ACE2 is seen as a “double-edged sword”<sup>10</sup>. While high expression of the receptor enables viral infection, some of the deleterious effects associated with COVID-19 are attributed to loss of ACE2-mediated cardiovascular protection, due to cell surface downregulation<sup>11</sup>. In the current COVID-19 pandemic, there has been great interest in novel therapeutics that modulate ACE2, either to prevent SARS-CoV-2 entry<sup>12</sup> or to target the renin-angiotensin system imbalance associated with severe disease<sup>11</sup>. Ideally, novel ACE2-focused therapies should be able to disentangle these two faces of the receptor.

The gamma-secretase ( $\gamma$ S) protein complex, composed of a Presenilin 1/2 aspartyl protease catalytic core with regulatory (Aph-1a or -1b), enhancer (PEN2) and targeting (Nicastrin) subunits, is the prototype intramembrane-cleaving protease (I-CLiP). I-CLiP proteases introduce a water molecule into the hydrophobic environment of the lipid bilayer for peptide bond hydrolysis within the transmembrane domain.  $\gamma$ S targets are typically single-pass, type I transmembrane proteins with large ectodomains and C-terminal intracellular domains (ICD).  $\gamma$ S substrates first undergo ectodomain shedding at the cell surface, rendering a membrane-bound protein stub that is targeted by  $\gamma$ S for intramembrane proteolysis. The released soluble ICD tends to be rapidly degraded by the proteasome, but in some cases, such as the Notch family of cell surface receptors<sup>13</sup> and the amyloid  $\beta$  precursor protein (APP)<sup>14</sup>, the ICD has signaling activity. For example, Notch ICD binds a Mastermind/Rbpj complex to activate transcription of canonical Notch target genes<sup>15</sup>. But in addition to Notch and APP, dozens of other putative  $\gamma$ S targets have been identified<sup>16</sup>, not determined by an amino acid consensus sequence, but rather specific transmembrane conformational structure and accessibility<sup>17,18</sup>. Validation of novel  $\gamma$ S targets is hindered by the lack of clear-cut common features and ectodomain shedding requirements.

Based on structural similarity of ACE2 to known  $\gamma$ S targets, we hypothesized that  $\gamma$ S regulates intramembrane cleavage of ACE2 and may impact SARS-CoV-2 biology. Here we report that ACE2 undergoes TMPRSS2/ADAM17-dependent  $\gamma$ S cleavage, resulting in a short-lived ACE2-ICD. Genetic or chemical inhibition of  $\gamma$ S prevents ACE2-ICD generation, leading to accumulation of a membrane-bound ACE2 lacking the ectodomain. However, we show using a pseudovirus system that  $\gamma$ S inhibition does not impact SARS-CoV-2 cellular entry.

<sup>1</sup>Department of Medicine, Columbia University Irving Medical Center, New York, NY, USA. <sup>2</sup>Aaron Diamond AIDS Research Center, Columbia University Irving Medical Center, New York, NY, USA. ✉email: up2104@cumc.columbia.edu



◀ **Figure 1.** ACE2 is targeted by  $\gamma$ S after ectodomain shedding. **(A)** Schematic and scaled representation of  $\gamma$ S targets JAGGED1 or NOTCH1, with ACE2, ACE2-C9 and ACE2-GFP. Domains and regions targeted by sheddases are depicted. Predicted molecular weight of ACE2 $\Delta$ E after TMPRSS2/ADAM17-mediated cleavage is shown. **(B)** Western blots from 293 T cells transfected with ACE2-C9 with or without TMPRSS2, then treated with DBZ (dibenzazepine 100 nM) (+), or DMSO (-). Mobility consistent with full length (FL) and ACE2 lacking its ectodomain (ACE2 $\Delta$ E) indicated. ACE2 $\Delta$ E generated in the absence of TMPRSS2 has a higher molecular weight, which corresponds to ADAM17-mediated shedding. **(C)** Western blots from 293 T cells transfected with ACE2-C9 with or without PMA (200 nM, 15 h) treatment. **(D)** Western blots from 293 T cells transfected with ACE2-C9, with or without TMPRSS2, or treated with PMA, with or without two  $\gamma$ S inhibitors [DBZ (dibenzazepine, 100 nM) or CmpE (compound E, 40 nM)]. **(E)** Western blots from 293 T cells transfected with ACE2-GFP, with or without TMPRSS2, then treated with DBZ and/or MG132 (1  $\mu$ M, 15 h). **(F)** Western blots from 293 T cells transfected with ACE2-GFP, with or without PMA, DBZ and/or MG132. **(G)** Western blots from immunoprecipitates derived from 293 T cells transfected with ACE2-C9, with or without TMPRSS2, then treated with DBZ. Data is representative of 2–3 independent experiments.

## Results

**ACE2 ectodomain shedding is required for  $\gamma$ S cleavage.** Consistent with other confirmed  $\gamma$ S targets (i.e. APP<sup>14</sup>, Notch<sup>13</sup> and Jagged1<sup>19</sup>), ACE2 has a large ectodomain that can be processed by a sheddase (ADAM17/TMPRSS2)<sup>5,6</sup> and a single transmembrane domain (Fig. 1A). Based on this structural similarity, we hypothesized that after ectodomain shedding, the resultant protein (ACE2 $\Delta$ E) may represent a novel  $\gamma$ S target. To test this hypothesis, we expressed ACE2 tagged at its C-terminus in 293 T cells, and triggered ectodomain shedding by either TMPRSS2 co-expression, or PMA-induced activation of endogenous sheddases<sup>20</sup>. In the presence of TMPRSS2, we observed a 15 kDa C-terminal ACE2 fragment which accumulated in the presence of a  $\gamma$ S inhibitor (GSI), dibenzazepine (DBZ) (Fig. 1B). PMA treatment rendered a 18 kDa C-terminal fragment, consistent with the expected size after ADAM17-mediated ACE2 cleavage<sup>6</sup>. Similar to TMPRSS2 co-expression, this longer form of ACE2 $\Delta$ E also accumulated in DBZ treated cells (Fig. 1C). Intriguingly, we observed ACE2 $\Delta$ E accumulation even in unstimulated cells expressing ACE2 (Fig. 1B,C), suggesting endogenous ectodomain shedding followed by  $\gamma$ S cleavage is part of the normal turnover of ACE2. We also used a chemically distinct GSI (Compound E) (Fig. 1D), that confirmed that ACE2 $\Delta$ E is targeted by  $\gamma$ S.

Most  $\gamma$ S-liberated target protein ICDs are extremely labile and rapidly degraded in the proteasome<sup>16</sup>. As the cytoplasmic portion of ACE2 is too small for conventional SDS-PAGE, we generated a C-terminal ACE2-GFP fusion protein to detect ACE2-ICD production. We repeated the above experiments using this novel construct and found that TMPRSS2 co-expression or PMA treatment provoked ectodomain shedding and ACE2 $\Delta$ E-GFP accumulation with DBZ treatment (Fig. 1E,F). As hypothesized, we also observed ACE2-ICD-GFP only after proteasome inhibition (Fig. 1E,F).

Based on these pharmacologic data, we next hypothesized that ACE2 $\Delta$ E and  $\gamma$ S would physically interact. To test this, we performed co-immunoprecipitation of endogenous  $\gamma$ S with C-terminally tagged ACE2, and observed association with both Nicastrin and Presenilin1 with ACE2 $\Delta$ E but not full-length ACE2, consistent with other *bona fide*  $\gamma$ S targets<sup>18</sup>.  $\gamma$ S-ACE2 $\Delta$ E interaction did not change in the presence of DBZ (Fig. 1G). In sum, these data establish ACE2 as a novel  $\gamma$ S target.

**ACE2 cleavage-dependent localization is altered in  $\gamma$ S-deficient cells.** To determine cellular ramifications of  $\gamma$ S-mediated ACE2 cleavage, we next evaluated ACE2 processing in Nicastrin knockout (Ncstn KO)<sup>21</sup> or Presenilin1/2 double knockout (Psen1/2 dKO) MEFs<sup>22</sup>, both of which have disrupted  $\gamma$ S activity. Consistent with GSI treatment, these  $\gamma$ S-deficient cell lines displayed ACE2 $\Delta$ E accumulation, accentuated by co-expression of TMPRSS2 (Fig. 2A). In this experimental paradigm, the C-terminus of ACE2 is primarily localized to the membrane but appeared diffusely cytoplasmic with TMPRSS2 expression in control cells (Fig. 2B and 2C, top panels). In  $\gamma$ S-deficient cells however, ACE2 remained membrane-associated even in the presence of TMPRSS2 (Fig. 2B,C, bottom panels). We reproduced these results using a C-terminal ACE2-GFP fusion protein (Fig. 2D), and with DBZ treatment of  $\gamma$ S in control cells (Fig. 2E). These results indicate that  $\gamma$ S is required for the release of a soluble C-terminal ACE2 fragment from cell membranes.

**Endogenous ACE2 cleavage is regulated by  $\gamma$ S.** 293 T and MEFs do not express significant levels of endogenous ACE2. To confirm the physiologic relevance of  $\gamma$ S-mediated ACE2 cleavage, we used two well-characterized ACE2-positive cell lines that allow SARS-CoV-2 infection and replication, Caco-2 and VeroE6. Using an antibody that recognizes the C-terminal region of ACE2, we observed accumulation of endogenous ACE2 $\Delta$ E with GSI treatment in both cell lines (Fig. 3A–C). These data confirmed results from ectopic ACE2 expression, using endogenous ACE2 and TMPRSS2/ADAM17 (in Caco-2 cells) or ADAM17 alone (in VeroE6), leading to the expected ACE2 $\Delta$ E product of ADAM17-mediated cleavage. We next took advantage of this system to test whether longer ACE2 $\Delta$ E half-life or impaired production of ACE2-ICD may produce negative feedback on this pathway in these cells. This hypothesis was based on nuclear localization and transcriptional activity of the C-terminal fragment of the related protein, ACE<sup>23,24</sup>. However, we did not observe nuclear ACE2 or differences in expression of ACE2, TMPRSS2 or ADAM17 in DBZ-treated VeroE6 or Caco-2 cells (Fig. 3D,E). These data render unlikely the possibility that ACE2-ICD mediates feedback inhibition on ACE2 gene expression.

**$\gamma$ S inhibition does not alter SARS-CoV-2 S-protein-mediated cell entry.** As genetic or pharmacologic  $\gamma$ S inhibition affected ACE2 cleavage and subcellular localization, we hypothesized that GSI may reduce

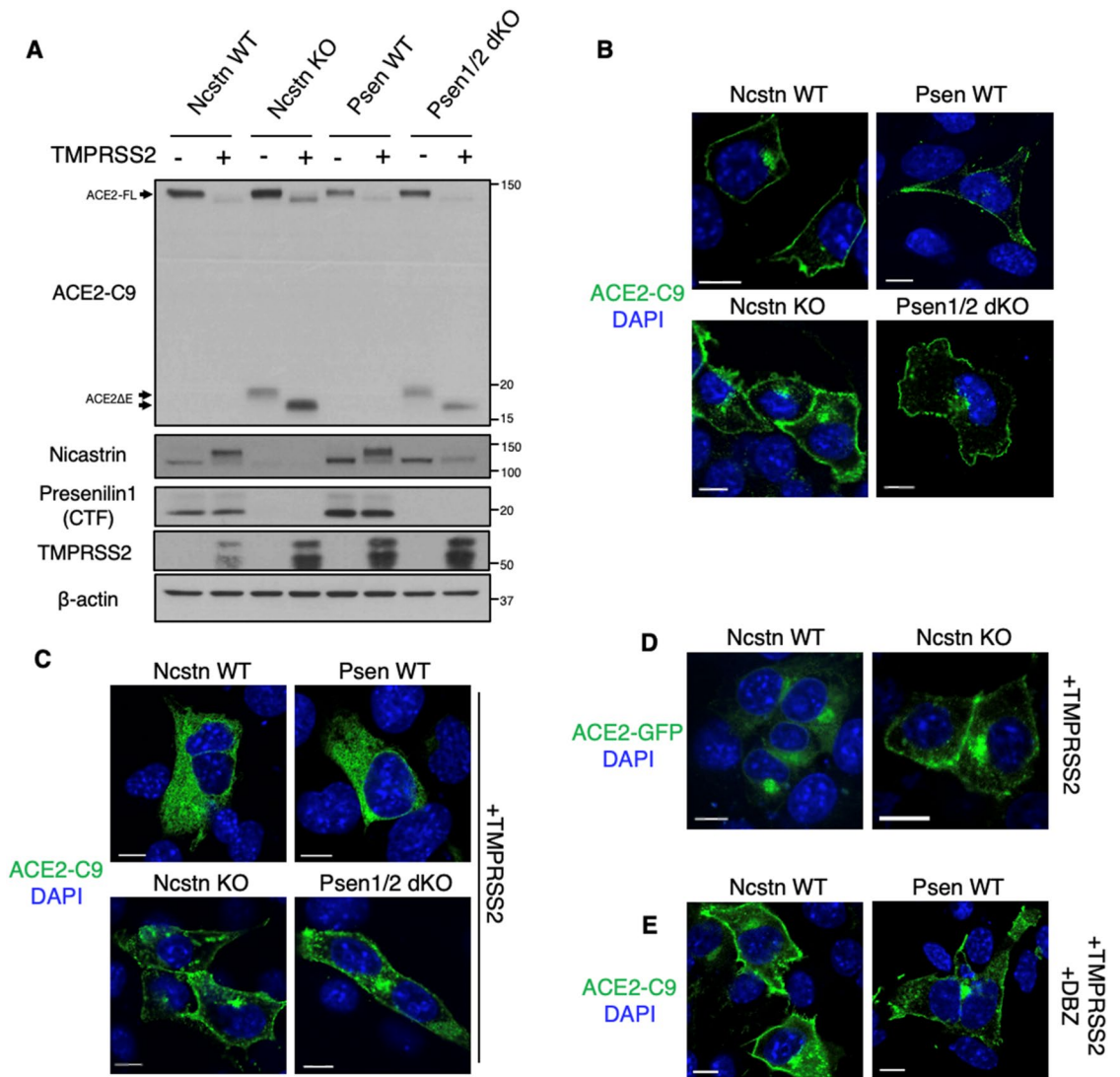


**Figure 2.**  $\gamma$ S-deficient cells cannot process ACE2 $\Delta$ E. (A) Western blots from Presenilin 1/2 double KO (Psen1/2 dKO) or Nicastrin KO (Ncstn KO) MEFs and their wild type (WT) controls. Cells were transfected with ACE2-C9 with or without TMPRSS2. ACE2 $\Delta$ E generated in the absence of TMPRSS2 has a higher molecular weight, which corresponds to ADAM17-mediated shedding. (B) Representative immunofluorescence images of WT MEFs transfected with ACE2-C9. (C) Representative immunofluorescence images of WT, Psen1/2 dKO and Ncstn KO MEFs transfected with ACE2-C9 and TMPRSS2. (D) GFP fluorescence in WT or Ncstn KO MEFs co-expressing ACE2-GFP and TMPRSS2. (E) Representative immunofluorescence images of WT MEFs transfected with ACE2-C9 and TMPRSS2 in the presence of GSI. Scale bars: 10  $\mu$ m.

SARS-CoV-2 cell entry and replication. To test this potential, we utilized SARS-CoV-2 S-protein pseudotyped with VSV and tested a wide range of DBZ concentrations (0.3 nM–1  $\mu$ M). In comparison to a potent S-protein neutralizing antibody, used as a positive control<sup>25</sup>, DBZ did not affect SARS-CoV-2 S-protein mediated viral entry in VeroE6 or in Caco-2 cells (Fig. 4). These results indicate that although  $\gamma$ S is necessary for ACE2 intracellular processing, blocking  $\gamma$ S does not affect viral entry.

## Discussion

ACE2 has recently caught the attention of the research community because of its role as the functional receptor of SARS-CoV-2<sup>3</sup>. Here we have characterized ACE2 as a novel target of  $\gamma$ S (Fig. 5). Similar to other known targets<sup>16–18</sup>, ectodomain shedding prompts  $\gamma$ S-mediated intramembrane cleavage to release soluble ACE2-ICD. Some ICDs (i.e. Notch) generated by  $\gamma$ S are transcriptionally active, but a functional role of many others remains elusive<sup>16</sup>.  $\gamma$ S has also been dubbed as the “proteasome of the membrane”<sup>26</sup>. Our finding that ACE2-ICD is rapidly cleared by proteasomal degradation suggests is consistent with the view that  $\gamma$ S-mediated cleavage represents a way to dispose membrane proteins stubs. However, our data cannot as yet discard the hypothesis that ACE2-ICD might represent a novel biologically active peptide.

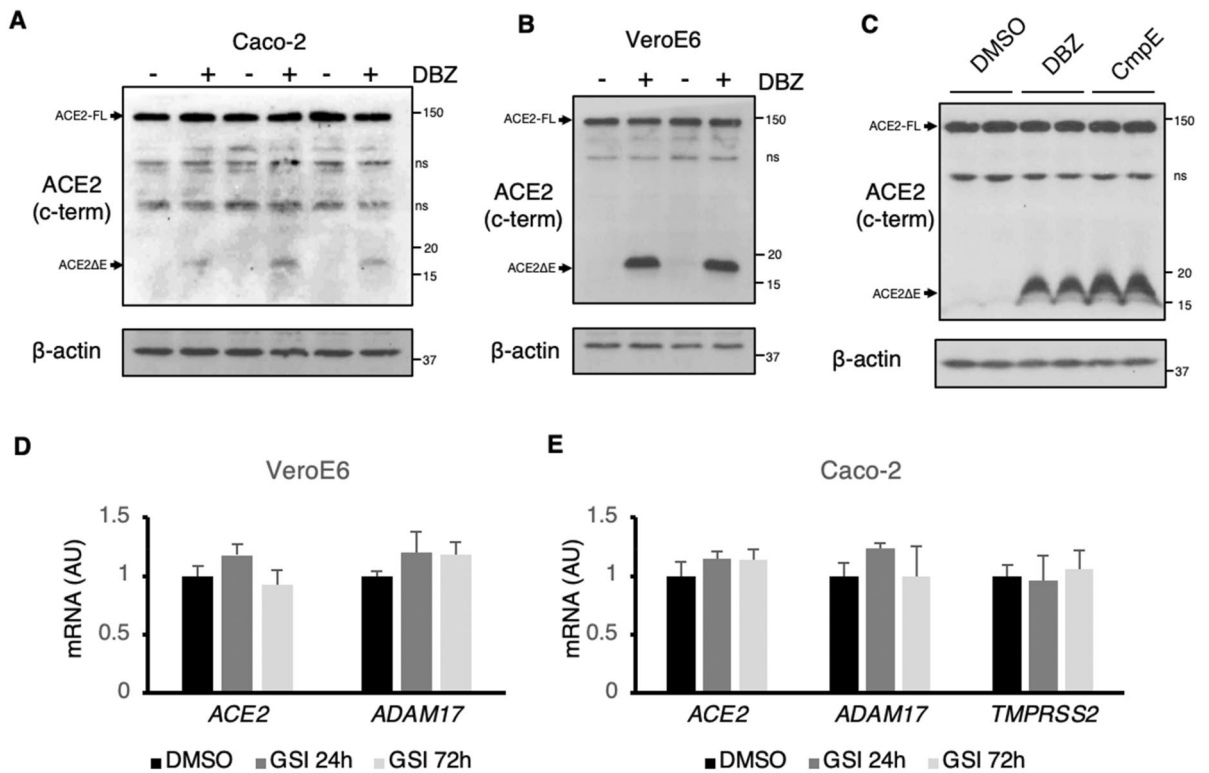


**Figure 3.**  $\gamma$ S inhibition targets endogenous ACE2. (A) Western blots of Caco-2 cells treated with DBZ (+) or DMSO (-). (ns) indicates non-specific bands. (B) Western blots of VeroE6 cells treated with DBZ (+) or DMSO (-). (C) Western blots of VeroE6 cells treated with DBZ compound E (CmpE) or DMSO (-). D, Gene expression in VeroE6 after 24 or 72 h treatment with DBZ, showing means  $\pm$  SD. (E) Gene expression in Caco-2 cells after 24 or 72 h treatment with DBZ, showing means  $\pm$  SD.

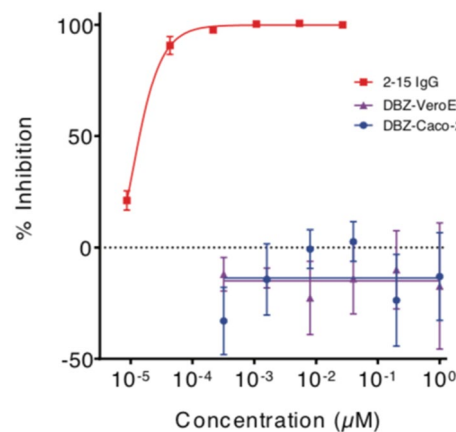


**Figure 4.**  $\gamma$ S inhibition does not prevent SARS-CoV-2 S-protein mediated cell entry. Inhibition of SARS-CoV-2 pseudovirus by DBZ at the indicated concentrations tested on VeroE6 or Caco-2 cells. A SARS-CoV-2 neutralizing antibody, 2-15, tested on VeroE6 was used as a positive control. Triplicates are presented as means  $\pm$  SEM.

Previous reports indicate that ACE2 processing by cell membrane proteases such as ADAM17 or TMPRSS2 impacts SARS-CoV S-protein mediated cell entry<sup>5,7</sup>. Our data is clear that pharmacologic inhibition of  $\gamma$ S-mediated ACE2 cleavage does not, but cannot rule out the possibility that other compounds termed “ $\gamma$ S modulators” (GSMs)<sup>27</sup> may behave differently. GSMs, developed primarily to differentially affect  $\gamma$ S processing of so-called “on-target” (i.e. APP) as opposed to “off-target” (i.e. Notch) substrates, may in fact selectively increase  $\gamma$ S processivity. In light of our finding that ACE2 is a novel  $\gamma$ S target, GSMs are worth evaluating for

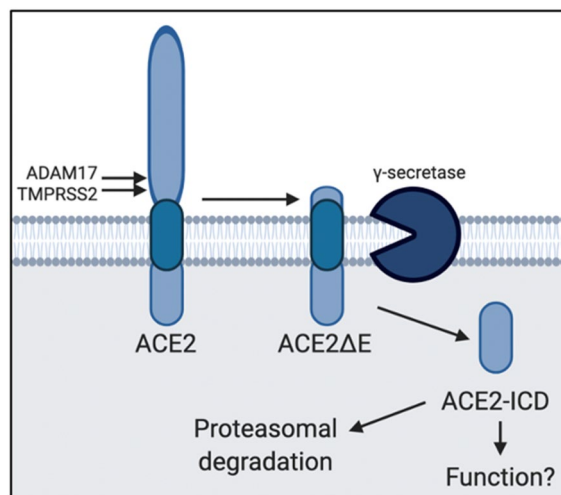


**Figure 5.** Model of ACE2 cleavage. Model showing the sequential processing of full length ACE2 by ADAM17/TMPRSS2 and  $\gamma$ S, rendering ACE2 $\Delta$ E and ACE2-ICD, respectively. ACE2-ICD is then rapidly degraded in the proteasome. The functional consequence of ACE2-ICD is not yet known.

biological activity against SARS-CoV-2 pathogenesis. In addition, some groups have speculated that blocking Notch signaling with GSIs may ameliorate COVID-19 progression<sup>28</sup>. Notch signaling promotes M1 polarization of macrophages<sup>29</sup>, and also contributes to T-cell cytokine production<sup>30</sup>. Thus, despite our finding that GSI does not directly affect viral entry, potential effects to block Notch-induced hyperinflammation suggest compounds that have completed Ph2/3 clinical trials can potentially be repurposed for COVID-19.

In addition to the relatively recently discovered role as a viral receptor, ACE2 has known roles in the renin-angiotensin system<sup>31</sup>, but also other potential functions. For example, mutations causal of Hartnup disorder impair association of the neutral amino acid transporter SLC6A19 with ACE2, suggesting that ACE2 serves as a chaperone for membrane trafficking<sup>32</sup>, akin to the function of collectrin towards SLC6A19 or SLC1A1<sup>33</sup>. It is possible that  $\gamma$ S-mediated transmembrane processing of ACE2 may impact ACE2 chaperone ability, or even in the structurally homologous collectrin. These potential ramifications of our findings require further study.

In sum, our results demonstrate that ACE2 is a novel  $\gamma$ S target, but that pharmacologic inhibition of  $\gamma$ S does not impact SARS-CoV-2 S-protein mediated cell entry. Given the pharmacologic accessibility of  $\gamma$ S, with prior evaluation of GSIs and GSMs for Alzheimer's Disease and cancer, we present these data to encourage further exploration into this novel biology for application to COVID-19 or to other pathology attributable to the myriad functions ascribed to ACE2.

## Methods

**Antibodies and chemicals.** Antibodies against GFP (B-2) sc-9996, Nicastrin (N-19) sc-14369, TMPRSS2 (H-4) sc-515727, Rhodopsin (ID4) sc-57432, C9 tag (TETSQVAPA peptide) were from Santa Cruz Biotechnology; Actin, A2066 from Millipore-Sigma; Presenilin 1-carboxy terminal fragment (CTF) (D39D1) 5643, from Cell Signaling Technology; and ACE2 ab15348, from Abcam. MG132 and phorbol 12-myristate 13-acetate (PMA) (Sigma).  $\gamma$ S inhibitors (GSI) used were Compound E (Axxora) and dibenzazepine (DBZ) (Syncom).

**Cell culture and cell lines.** Presenilin-deficient (Psen1/2 double knockout) and control mouse embryonic fibroblasts (MEFs) were provided by Nikolaos Robakis (Mount Sinai School of Medicine, New York, NY)<sup>22</sup> and Nicastrin knockout and control MEFs were obtained from Phillip Wong (Johns Hopkins University School of Medicine, Baltimore, MD)<sup>21</sup>. MEFs, Caco-2, VeroE6 and 293 T cells were cultured in DMEM supplemented with 10% heat-inactivated fetal bovine serum (FBS) and 1% penicillin-streptomycin (Thermo-Fisher). For transfection experiments, Lipofectamine 3000 and OptiMEM were used (Thermo-Fisher) as per the manufacturer's instructions.

**Plasmids.** C-terminally tagged ACE2 (TETSQVAPA, C9-tag) from Hyeryun Choe, was obtained from Addgene (#1786)<sup>2</sup>. C9 was replaced with EGFP to generate ACE2-GFP, which was in turn deposited to Addgene (#154962). TMPRSS2 expression vector from Roger Reeves, was obtained from Addgene<sup>34</sup>.

**Western blotting, immunoprecipitation and quantitative PCR.** Cells were lysed in RIPA buffer containing protease inhibitors (Pierce protease inhibitor tablets, Thermo-Fisher), and 10 mM NaF. For immunoprecipitation of  $\gamma$ S, cells were lysed in 1% CHAPSO, 100 mM NaCl, 2 mM EDTA, 25 mM Tris-HCl (pH 7.4), with protease inhibitors, and 1.2 mg of protein lysate immunoprecipitated with 2.5  $\mu$ g C9-tag antibody and Protein G magnetic beads (Cell Signaling Biotechnology). After overnight incubation, beads were separated with a DynaMag-2 magnet (Thermo-Fisher), and washed three times in buffer containing 0.5% CHAPSO. Beads

were re-suspended in 2× Laemmli buffer and heated at 70°C for 10 min, prior to SDS-PAGE, Western blot and visualization with the ECL Western Blotting Detection Kit (GE Healthcare Bio-Sciences). Uncropped original scans of blots are shown in Supplementary Information.

qPCR was performed as previously described<sup>35</sup> with primers specific for human (h) Caco-2 cells; or *Chlorocebus sabaues* (cs) VeroE6 cells as follows: *h/csACE2*: TGGTGGGAGATGAAGCGAGA, AACATGGAACAGAGATGCGGG; *h/TMPRSS2*: CACCGAGGAGAAAGGGAAGAC, CATGGCTGGTGTGATCAGGT; *csADAM17*: AGGTGTCCAGTGCAGTGATAGG, ATCTTCAGCATTTCCTCGGAGG; *hADAM17*: CGTTGGGTCTGTCTGGTTT, TCAGCATTTCGACGTTACTGGG. qPCR results were normalized with peptidylprolyl isomerase A using the following primers: *csPPIA*: CAGGTCCTGGCATCTTGTC, GCTTGCCATCCAACCACTCA; *hPPIA*: TATCTGCACTGCCAAGACTGAGTG, CTTCTTGCTGGTCTTGCCATTCC.

**Immunofluorescence and confocal imaging.** Cells were seeded on glass coverslips as previously described<sup>36</sup>, and images gathered with an Axio Observer Z1 with an LSM 710 scanning module (Zeiss), collected using a 63× Zeiss Plan-Apochromat oil objective. All images were obtained in a 1024- by 1024-pixel format and processed with ZEN2 (Zeiss).

**SARS-CoV-2 pseudovirus and cell entry inhibition.** Recombinant Indiana vesicular stomatitis virus (rVSV) expressing SARS-CoV-2 S-protein, and the neutralizing antibody used as control, were generated as described<sup>25</sup>. 293 T cells were grown to 80% confluency before transfection with pCMV3-SARS-CoV-2-spike using FuGENE 6 (Promega), and cultured overnight at 37 °C with 5% CO<sub>2</sub>. The next day, medium was removed and cells were infected with VSV-G pseudo-typed ΔG-luciferase (G\*ΔG-luciferase, Kerafast) in DMEM at an MOI of 3 for 1 h before washing the cells with 1× DPBS three times. DMEM supplemented with anti-VSV-G antibody (I1, mouse hybridoma supernatant from CRL-2700; ATCC) was added to the infected cells, and supernatant harvested the next day. To test DBZ inhibition of SARS-CoV-2 cell entry, VeroE6 or Caco-2 cells were seeded in a 96-well plate at a concentration of 2× 10<sup>4</sup> cells per well. Pseudovirus were incubated the next day with serial dilutions of DBZ in triplicate for 30 min at 37 °C. The mixture was added to cultured cells and incubated for an additional 24 h. An S-protein neutralizing antibody was used as control<sup>25</sup>. Luminescence was measured using a Britelite plus Reporter Gene Assay System (PerkinElmer) (Suppl. Information).

Received: 25 September 2020; Accepted: 21 April 2021

Published online: 07 May 2021

## References

- Hofmann, H. *et al.* Human coronavirus NL63 employs the severe acute respiratory syndrome coronavirus receptor for cellular entry. *Proc. Natl. Acad. Sci. USA* **102**, 7988–7993 (2005).
- Li, W. *et al.* Angiotensin-converting enzyme 2 is a functional receptor for the SARS coronavirus. *Nature* **426**, 450–454 (2003).
- Hoffmann, M. *et al.* SARS-CoV-2 cell entry depends on ACE2 and TMPRSS2 and is blocked by a clinically proven protease inhibitor. *Cell* **181**, 271–280.e8 (2020).
- Glowacka, I. *et al.* Evidence that TMPRSS2 activates the severe acute respiratory syndrome coronavirus spike protein for membrane fusion and reduces viral control by the humoral immune response. *J. Virol.* **85**, 4122–4134 (2011).
- Heurich, A. *et al.* TMPRSS2 and ADAM17 cleave ACE2 differentially and only proteolysis by TMPRSS2 augments entry driven by the severe acute respiratory syndrome coronavirus spike protein. *J. Virol.* **88**, 1293–1307 (2013).
- Lambert, D. W. *et al.* Tumor necrosis factor-α convertase (ADAM17) mediates regulated ectodomain shedding of the severe-acute respiratory syndrome-coronavirus (SARS-CoV) receptor, angiotensin-converting enzyme-2 (ACE2). *J. Biol. Chem.* **280**, 30113–30119 (2005).
- Haga, S. *et al.* Modulation of TNF-α-converting enzyme by the spike protein of SARS-CoV and ACE2 induces TNF-α production and facilitates viral entry. *Proc. Natl. Acad. Sci. USA* **105**, 7809–7814 (2008).
- Wang, S. *et al.* Endocytosis of the receptor-binding domain of SARS-CoV spike protein together with virus receptor ACE2. *Virus Res.* **136**, 8–15 (2008).
- Oudit, G. Y. *et al.* SARS-coronavirus modulation of myocardial ACE2 expression and inflammation in patients with SARS. *Eur. J. Clin. Invest.* **39**, 618–625 (2009).
- Touyz, R. M., Li, H. & Delles, C. ACE2 the Janus-faced protein—From cardiovascular protection to severe acute respiratory syndrome-coronavirus and COVID-19. *Clin. Sci.* **134**, 747–750 (2020).
- Liu, P. P., Blet, A., Smyth, D. & Li, H. The science underlying COVID-19. *Circulation* **142**, 68–78 (2020).
- Ragia, G. & Manolopoulos, V. G. Inhibition of SARS-CoV-2 entry through the ACE2/TMPRSS2 pathway: A promising approach for uncovering early COVID-19 drug therapies. *Eur. J. Clin. Pharmacol.* <https://doi.org/10.1007/s00228-020-02963-4> (2020).
- De Strooper, B. *et al.* A presenilin-1-dependent gamma-secretase-like protease mediates release of Notch intracellular domain. *Nature* **398**, 518–522 (1999).
- De Strooper, B. *et al.* Deficiency of presenilin-1 inhibits the normal cleavage of amyloid precursor protein. *Nature* **391**, 387–390 (1998).
- Fryer, C. J., Lamar, E., Turbachova, I., Kintner, C. & Jones, K. A. Mastermind mediates chromatin-specific transcription and turnover of the Notch enhancer complex. *Genes Dev.* **16**, 1397–1411 (2002).
- Haapasalo, A. & Kovacs, D. M. The many substrates of presenilin/γ-secretase. *J. Alzheimers Dis.* **25**, 3–28 (2011).
- Struhl, G. & Adachi, A. Requirements for presenilin-dependent cleavage of notch and other transmembrane proteins. *Mol. Cell* **6**, 625–636 (2000).
- Bolduc, D. M., Montagna, D. R., Gu, Y., Selkoe, D. J. & Wolfe, M. S. Nicastrin functions to sterically hinder γ-secretase–substrate interactions driven by substrate transmembrane domain. *Proc. Natl. Acad. Sci. USA* **113**, E509–E518 (2016).
- LaVoie, M. J. & Selkoe, D. J. The Notch ligands, Jagged and Delta, are sequentially processed by alpha-secretase and presenilin/gamma-secretase and release signaling fragments. *J. Biol. Chem.* **278**, 34427–34437 (2003).
- Arribas, J. *et al.* Diverse cell surface protein ectodomains are shed by a system sensitive to metalloprotease inhibitors. *J. Biol. Chem.* **271**, 11376–11382 (1996).

21. Li, T., Ma, G., Cai, H., Price, D. L. & Wong, P. C. Nicastrin is required for assembly of presenilin/gamma-secretase complexes to mediate Notch signaling and for processing and trafficking of beta-amyloid precursor protein in mammals. *J. Neurosci.* **23**, 3272–3277 (2003).
22. Barthet, G. *et al.* Inhibitors of  $\gamma$ -secretase stabilize the complex and differentially affect processing of amyloid precursor protein and other substrates. *FASEB J.* **25**, 2937–2946 (2011).
23. Ignjacev-Lazich, I. *et al.* Angiotensin-converting enzyme regulates bradykinin receptor gene expression. *Am. J. Physiol. Heart Circ. Physiol.* **289**, H1814–H1820 (2005).
24. Lucero, H. A., Kintsurashvili, E., Marketou, M. E. & Gavras, H. Cell signaling, internalization, and nuclear localization of the angiotensin converting enzyme in smooth muscle and endothelial cells. *J. Biol. Chem.* **285**, 5555–5568 (2010).
25. Liu, L. *et al.* Potent neutralizing antibodies against multiple epitopes on SARS-CoV-2 spike. *Nature* **584**, 450–456 (2020).
26. Kopan, R. & Ilgan, M. X. G. Gamma-secretase: Proteasome of the membrane?. *Nat. Rev. Mol. Cell Biol.* **5**, 499–504 (2004).
27. Golde, T. E., Koo, E. H., Felsenstein, K. M., Osborne, B. A. & Miele, L.  $\gamma$ -Secretase inhibitors and modulators. *Biochim. Biophys. Acta* **1828**, 2898–2907 (2013).
28. Rizzo, P. *et al.* COVID-19 in the heart and the lungs: could we ‘Notch’ the inflammatory storm? *Basic Res. Cardiol.* 1–8. <https://doi.org/10.1007/s00395-020-0791-5> (2020).
29. Xu, H. *et al.* Notch-RBP-J signaling regulates the transcription factor IRF8 to promote inflammatory macrophage polarization. *Nat. Immunol.* **13**, 642–650 (2012).
30. Amsen, D., Helbig, C. & Backer, R. A. Notch in T cell differentiation: All things considered. *Trends Immunol.* **36**, 802–814 (2015).
31. Kuba, K., Imai, Y., Ohto-Nakanishi, T. & Penninger, J. M. Trilog of ACE2: A peptidase in the renin-angiotensin system, a SARS receptor, and a partner for amino acid transporters. *Pharmacol. Ther.* **128**, 119–128 (2010).
32. Kowalczyk, S. *et al.* A protein complex in the brush-border membrane explains a Hartnup disorder allele. *FASEB J.* **22**, 2880–2887 (2008).
33. Danilczyk, U. *et al.* Essential role for collectrin in renal amino acid transport. *Nature* **444**, 1088–1091 (2006).
34. Edie, S. *et al.* Survey of human chromosome 21 gene expression effects on early development in *Danio rerio*. *G3* **8**, 2215–2223 (2018).
35. Bartolomé, A., Zhu, C., Sussel, L. & Pajvani, U. B. Notch signaling dynamically regulates adult  $\beta$  cell proliferation and maturity. *J. Clin. Invest.* **129**, 268–280 (2019).
36. Bartolomé, A. *et al.* MTORC1 regulates both general autophagy and mitophagy induction after oxidative phosphorylation uncoupling. *Mol. Cell Biol.* **37**, e00441–e517 (2017).

## Acknowledgements

We thank Michael Yin, and members of the Pajvani and Ho laboratories for insightful discussion. Supported by NIH DK103818 (UBP) and a Russell Berrie Foundation Fellowship in Diabetes Research (AB). The content is solely the responsibility of the authors and does not necessarily represent the official views of the National Institutes of Health.

## Author contributions

A.B. designed, performed and interpreted experiments, and wrote the manuscript. J.L., P.W., and D.D.H performed and interpreted experiments. U.B.P. designed and interpreted experiments, and wrote the manuscript.

## Competing interests

The authors declare no competing interests.

## Additional information

**Supplementary Information** The online version contains supplementary material available at <https://doi.org/10.1038/s41598-021-89379-x>.

**Correspondence** and requests for materials should be addressed to U.B.P.

**Reprints and permissions information** is available at [www.nature.com/reprints](http://www.nature.com/reprints).

**Publisher’s note** Springer Nature remains neutral with regard to jurisdictional claims in published maps and institutional affiliations.



**Open Access** This article is licensed under a Creative Commons Attribution 4.0 International License, which permits use, sharing, adaptation, distribution and reproduction in any medium or format, as long as you give appropriate credit to the original author(s) and the source, provide a link to the Creative Commons licence, and indicate if changes were made. The images or other third party material in this article are included in the article’s Creative Commons licence, unless indicated otherwise in a credit line to the material. If material is not included in the article’s Creative Commons licence and your intended use is not permitted by statutory regulation or exceeds the permitted use, you will need to obtain permission directly from the copyright holder. To view a copy of this licence, visit <http://creativecommons.org/licenses/by/4.0/>.

© The Author(s) 2021